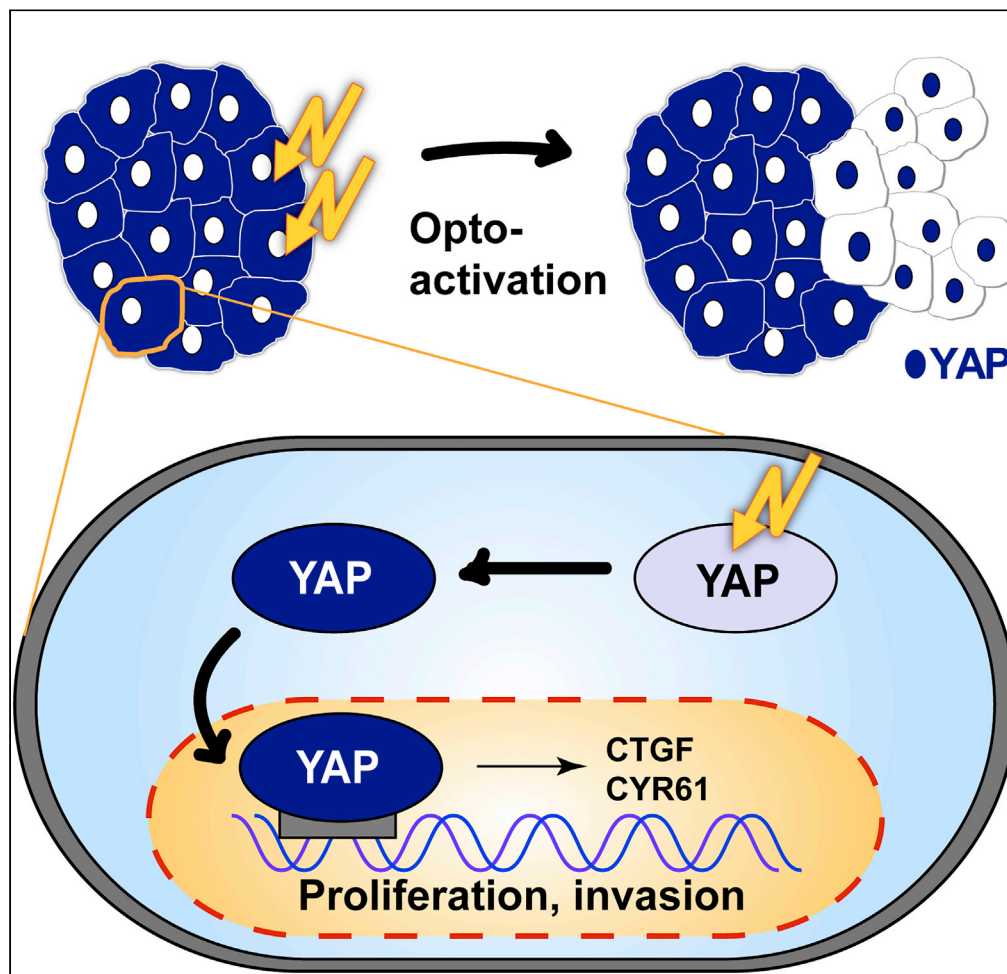


Article

Spatio-selective activation of nuclear translocation of YAP with light directs invasion of cancer cell spheroids



Bernhard Illies,
Adrian Fuchs,
Florian
Gegenfurtner,
Evelyn Ploetz,
Stefan Zahler,
Angelika M.
Vollmar, Hanna
Engelke

hanna.engelke@uni-graz.at

HIGHLIGHTS

Photoactivation of nuclear translocation of yes-associated protein (YAP)

Photoactivation of YAP induces downstream signaling

Site-selective activation of YAP triggers directed invasion of cancer spheroids

Illies et al., iScience 24, 102185
March 19, 2021 © 2021 The Authors.
<https://doi.org/10.1016/j.isci.2021.102185>



Article

Spatio-selective activation of nuclear translocation of YAP with light directs invasion of cancer cell spheroids

Bernhard Illies,¹ Adrian Fuchs,¹ Florian Gegenfurtner,² Evelyn Ploetz,¹ Stefan Zahler,² Angelika M. Vollmar,² and Hanna Engelke^{1,3,4,*}

SUMMARY

The mechanical properties of the extracellular matrix strongly influence tumor progression and invasion. Yes-associated protein (YAP) has been shown to be a key regulator of this process translating mechanical cues from the extracellular matrix into intracellular signals. Despite its apparent role in tumor progression and metastasis, it is not clear yet, whether YAP activation can actively trigger the onset of invasion. To address this question, we designed a photo-activatable YAP (optoYAP), which allows for spatiotemporal control of its activation. The activation mechanism of optoYAP is based on optically triggered nuclear translocation of the protein. Activation of optoYAP induces downstream signaling for several hours and leads to increased proliferation in two- and three-dimensional cultures. Applied to cancer spheroids, optoYAP activation induces invasion. Site-selective activation of optoYAP in cancer spheroids strikingly directs invasion into the activated direction. Thus, nuclear translocation of YAP may be enough to trigger the onset of invasion.

INTRODUCTION

Yes-associated protein (YAP) is a key regulator of mechanosignaling. It translates mechanical cues from the extracellular matrix into intracellular signals (Dupont et al., 2011). This process is mediated via its localization within the cell: YAP is cytoplasmic on soft substrates and translocates into the nucleus upon sensing mechanical forces, e.g., by a stiff substrate (Dupont et al., 2011; Elosegui-Artola et al., 2017). In the nucleus, it activates downstream signaling. High nuclear YAP has been shown to be associated with invasion and altered matrix properties in tumors (Zanconato et al., 2016; Lin et al., 2015). However, due to lack of control over its translocation, it is not clear whether nuclear YAP is sufficient to induce invasion or whether it is rather just associated with invasion. YAP is able to induce symmetry breaks in cell collectives (Serra et al., 2019). We therefore hypothesized that it may be responsible for triggering the symmetry break, which is essential for the occurrence of invasive buds of a tumor and, subsequently, invasion. For a test of this hypothesis, we needed a local activation of YAP to ensure a sufficiently asymmetrical cue that induces the symmetry break. To obtain the necessary spatiotemporal control of YAP's translocation into the nucleus, we developed an optical control of YAP's nuclear translocation (Valon et al., 2017).

RESULTS

Photoactivation of YAP

In the cell, localization of YAP is regulated by several different processes, and the exact regulation principles are not entirely known yet (Pocaterra et al., 2020). To keep the interference with other signaling processes low and maximize the amount of control, we prepend a small (20 amino acids) photo-controlled nuclear localization signal (optoNLS) (Engelke et al., 2014), which we developed earlier, to YAP resulting in a photo-activatable YAP (optoYAP). The optoNLS is based on genetic insertion of a photocaged lysine (Gautier et al., 2010) (Fig. S1, S2) into a nuclear localization signal, which blocks nuclear import entirely (Engelke et al., 2014). Uncaging the lysine with light yields the functional signal and restores nuclear import. The small size of optoNLS and caging group minimizes their impact on protein function. To visualize protein localization and block nuclear import via diffusion by an increase in size, we use a YAP fused to two enhanced green fluorescent proteins (eGFPs). To

¹Department of Chemistry and Center for NanoScience (CeNS), Ludwig-Maximilians-Universität München, Butenandtstraße 11, 81377 Munich, Germany

²Department of Pharmacy, Ludwig-Maximilians-Universität München, Butenandtstraße 5, 81377 Munich, Germany

³Institute of Pharmaceutical Sciences, Department of Pharmaceutical Chemistry, University of Graz, Humboldtstr. 46, 8010 Graz, Austria

⁴Lead contact

*Correspondence:

hanna.engelke@uni-graz.at
<https://doi.org/10.1016/j.isci.2021.102185>



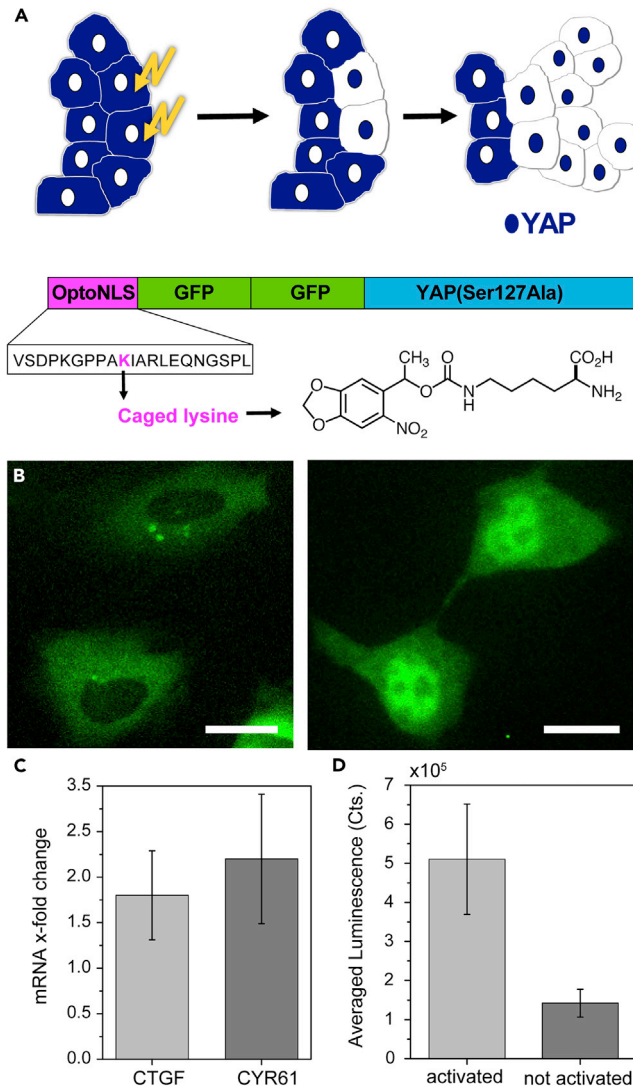


Figure 1. Photoactivation of YAP

(A) Schematics of optoYAP. OptoYAP is composed of the optoNLS with a caged lysine and two GFP prepended to YAP Ser127Ala. The optoNLS is activated by uncaging the lysine with light leading to nuclear localization of optoYAP followed by enhanced proliferation in the photo-activated area.

(B) HeLa cells transfected with optoYAP show YAP localization in the cytosol before activation. Approximately 30 min after photoactivation, optoYAP is localized in the nucleus. Scale bar = 30 μ m.

(C) qPCR shows an increase in RNA levels of YAP downstream proteins CTGF and CYR61 (with GAPDH as gatekeeper).

(D) Yap functionality assay based on a TEAD luciferase reporter shows four times higher activity in activated samples compared to controls, which were not activated, confirming increased YAP activity. Data in (C) and (D) are represented as mean \pm standard deviation.

See also related [Figures S1–S7](#)

improve YAP detection we used a stabilized form of YAP, S127A that does not affect YAP regulation by mechanical signals ([Figure 1A](#)).

[Figure 1B](#) shows images of optoYAP-transfected cells. YAP was kept cytosolic either by serum depletion or mechanically by keeping the cells on a soft matrigel substrate. Before illumination, the entire optoYAP signal is cytosolic. Less than an hour after photoactivation, most of the optoYAP signal is located in the nucleus. This successful photo-activated translocation occurred independently of whether serum depletion or matrigel was used to prime cytosolic YAP with natural signaling. After successful nuclear translocation, functionality tests were

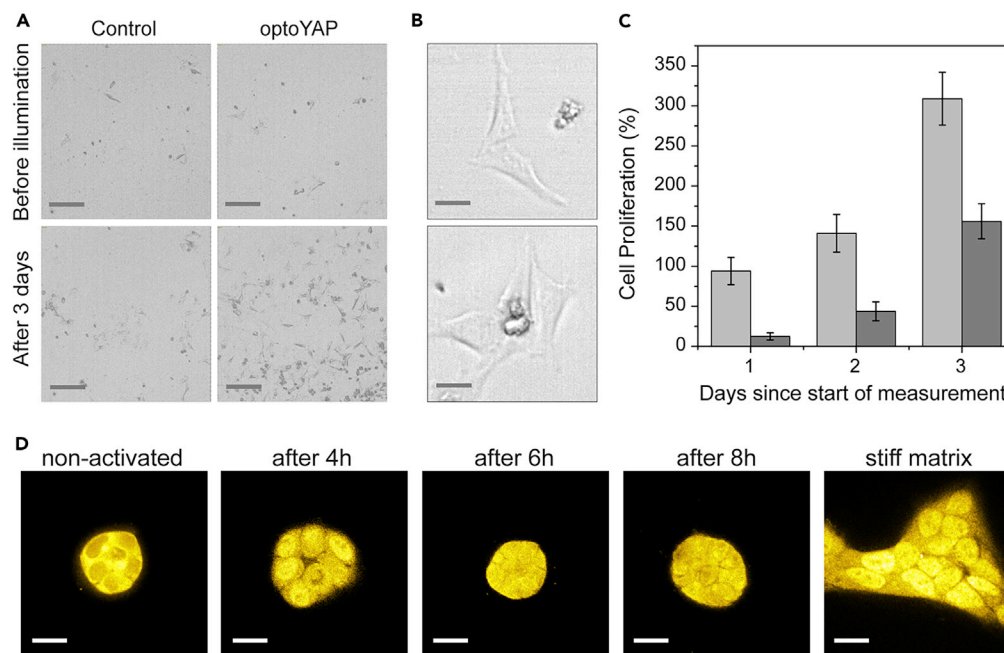


Figure 2. Proliferation and localization after optoYAP activation

(A) Proliferation of cells with optoYAP in FBS-depleted medium is strongly enhanced by photoactivation of optoYAP compared to controls without optoYAP. Scale bar: 200 μ m.

(B) Higher magnification images of cells in FBS-depleted medium show no changes in morphology after photoactivation. Scale bar: 20 μ m.

(C) Quantitative analysis of proliferation reveals a strong increase in the growth rate of photo-activated cells (light gray) compared to controls without optoYAP (dark gray) during the first day. This difference is amplified in the following days albeit at similar growth rates compared to the control. Note that growth rates on day 1 with activated optoYAP reach levels as known for proliferation under commonly used cell culture conditions (stiff substrate, medium supplemented with serum), which generally exhibit activated YAP. Data are represented as mean \pm standard deviation.

(D) Antibody staining of optoYAP transfected HeLa cells on matrigel before and after photoactivation. YAP is mainly cytosolic before activation; 4 h after activation it is located mainly in the nucleus, and at later time points, it returns to mainly cytosolic localization. For comparison, the nuclear localization of YAP in cells on a stiff matrix is shown. Scale bar: 20 μ m.

See also related [Figures S7–S12](#)

performed to show that optoYAP is fully functional and able to activate downstream signaling in the nucleus. quantitative PCR (qPCR) of CCN1 (CYR61) and CCN2 (CTGF)—proteins, which are upregulated downstream of YAP activation (Totaro et al., 2018)—reveals an enhanced signal compared to controls after photoactivation of YAP on an RNA level (Figure 1C). On a protein level, a luciferase reporter (Dupont et al., 2011) responsive to YAP signaling clearly showed enhanced expression (Figures 1D and S3) upon photoactivation of optoYAP revealing functional YAP-responsive signaling. Kinetics of YAP translocation as well as kinetics and size of downstream effects upon mechanical or chemical stimulation varies strongly depending on cell type, stimulation method, ratio of nuclear to cytosolic YAP before stimulation, and many other factors (Elosegui-Artola et al., 2017; Yu et al., 2012; Gegenfurtner et al., 2018). Kinetics of optoYAP translocation (Figures S4 and S5) and downstream effects (Figures 1C, 1D, and S3) are in the same range as measured for other stimuli (Yu et al., 2012). The absence of permanent DNA damage due to the illumination was also confirmed (Figures S6 and S7).

Proliferation after optoYAP activation

Having thus established a functional, photo-activatable YAP, we next studied the influence of YAP activation on HeLa cells cultured on two-dimensional substrates (Figures 2A and S8). Inactivation of YAP via serum depletion on plastic substrates did not change cell morphology. Accordingly, photoactivation of optoYAP did not lead to changes in cell morphology either (Figure 2B). However, proliferation was significantly increased: while the number of control cells without YAP activation increased after 24 h by 12.5% only, the number of cells after photoactivation of optoYAP was enhanced much stronger by 94% (Figure 2C). Note that cells with photo-activated YAP reach proliferation levels known for standard culture conditions

on a plastic substrate in a medium supplemented with serum, which induce active YAP. Cells with inactivated YAP proliferate much slower. Mechanical inactivation of YAP via growth on a soft matrigel substrate leads to a round cell morphology. Upon photoactivation of YAP, interestingly, cells did not change morphology to the stretched shape found on stiff substrates (Figure S9). However, similarly to serum-depleted, activated cells, they showed increased proliferation compared to controls resulting in enhanced growth of cell spheroids on the matrigel (Figure S10). Thus, the different cell morphologies on stiff and soft substrates, respectively, do not stem from the difference in YAP activation. The results rather suggest them to be a direct consequence of mechanical forces or other signaling pathways.

Kinetics of YAP localization and downstream signaling

To further understand the effect of the photo-activated YAP on cells, we investigated the time course of proliferation. Figure 2C already suggests the strongest effect of YAP to happen during the first day, which is then amplified by the exponential growth. A logarithmic plot and analysis (Figure S11) confirm that the growth rate of activated cells is enhanced during the first day and returns to non-activated levels on day 2 and thereafter. On a molecular level, we find an increased amount of nuclear YAP after activation. While nuclear YAP can be clearly seen 4 h after activation, the amount of nuclear YAP is decreased after 6 h (Figures 2D and S12). Finally, 8 h after activation it is almost back to cytosolic localization as in the non-activated state. A time course of the luciferase reporter assay also shows an increase in downstream signaling reaching a maximum around 4–6 h after illumination and decreasing afterward (Figure S3A). The time evolution of YAP's localization and downstream luciferase expression combined with the fact that proliferation is enhanced for one day suggests that activation of YAP as performed with our photoactivation induces a boost in downstream events, which lasts for several hours and vanishes over the course of a day.

YAP triggers directed growth in spheroids

Next, we investigated the effect of YAP activation on cell spheroids. To this end, spheroids were grown and embedded in collagen gels. In this three-dimensional model system, we also observed an increase in proliferation upon photoactivation of optoYAP in entire spheroids as shown in Figure 3A. Quantitative analysis (Figure 3B) reveals an increase in spheroid size by a factor of almost 4 (measured as the area of the z-projection including all connected invasive buds) over the course of three days after photoactivation of optoYAP, whereas controls hardly grew at all. Next to the enhanced size, YAP-activated spheroids also underwent morphological changes. YAP activation leads to an increased number of invading buds and network-like structures of invading cells as depicted in Figure 3A. These results already strongly suggest that activation of YAP can induce invasion.

Finally, we made use of the spatiotemporal control provided by the photoactivation. We used the spheroids in collagen gels and restricted optoYAP activation locally to a selected area of the spheroid. While non-activated controls grew symmetrically into all directions, strikingly, spatially selective activation of optoYAP was followed by invasion on the activated sites. Figure 3C shows the spherical non-illuminated spheroids and the invasive mass in the illuminated areas of photo-activated spheroids. Thus, local activation of YAP can induce a symmetry break and trigger invasion. Further microscopy studies of protein localization within the spheroids after photoactivation show the activated YAP 4 h after illumination (Figure 3D and see also Figure S13 for 3 days after illumination).

DISCUSSION

In conclusion, photoactivation of optoYAP in spheroids confirmed the hypothesis that YAP translocation into the nucleus is able to trigger invasion from the spheroids into the surrounding matrix. The results thus suggest YAP to be an important regulator of the onset of invasion. The developed optoYAP may also prove to be a useful tool for future investigations of the role of YAP in organ development, contact inhibition, and other processes in development and disease (Low et al., 2014).

Limitations of the study

As a tool, optoYAP is limited to irreversible activation due to the underlying photocleavage-based mechanism. Upon brief and non-toxic photoactivation (less than 1 min), it acts as “on-switch” of a functional YAP triggering downstream signaling for several hours with spatial control as provided by the light beam used for photoactivation. The temporal control is on the order of hours (30 min until full import, 8 h until recovery to mainly cytosolic YAP), which is not as fast as triggering YAP activation by applying force directly to the nucleus (Elosegui-Artola

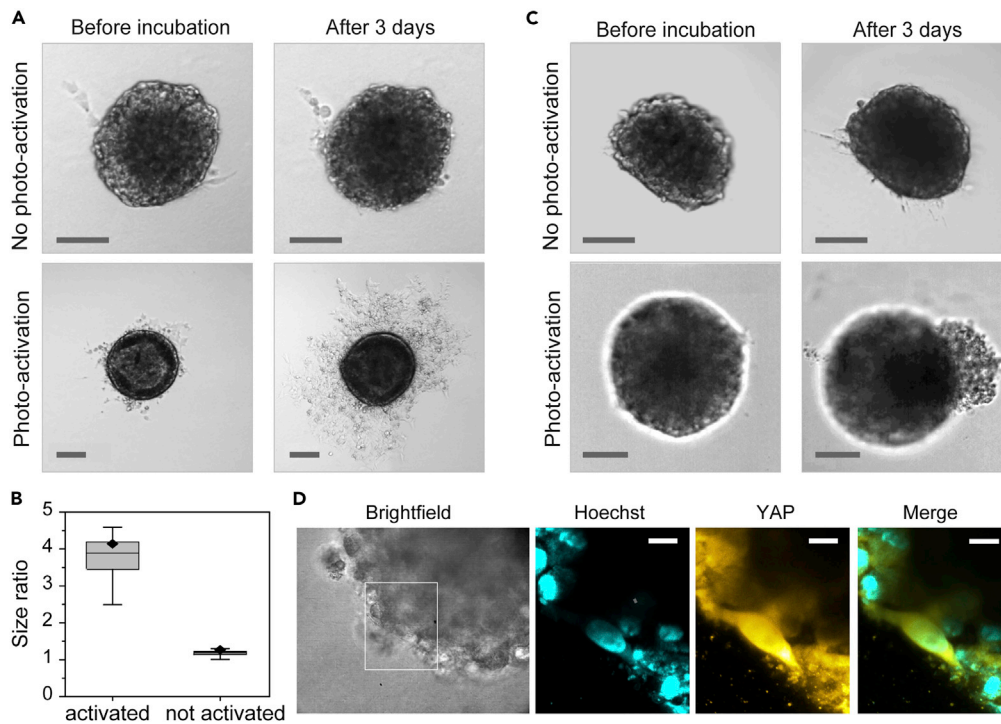


Figure 3. YAP triggers directed growth in spheroids

(A) HeLa spheroids in collagen gels transfected with optoYAP three days after photoactivation show increased invasion leading to a larger size of the spheroid compared to non-activated controls, which barely invade at all. Scale bars: 100 μm . (B) Quantification of the average spheroid size change over three days. Activated samples (light gray) show a fourfold increase in their size (measured as area of the central plane) over three days while non-activated samples (dark gray) grew only by a factor of 1.2. (C) Spatio-selective photoactivation of spheroids with optoYAP in collagen gels on the right side of the spheroid induces directed invasion on that side, while controls, which were not photo-activated, do not show directed growth. Scale bars: 100 μm . (D) High resolution and fluorescence imaging of activated YAP in a cell in a spheroid. Scale bars: 5 μm . See also related [Figures S13–S15](#).

[et al., 2017](#)), but fast enough given the timescales of downstream events and the timescales of processes in development and diseases such as the described invasion. The optoYAP construct is still sensitive to other physiological stimuli. Thus, the efficiency of photoactivation strongly depends on depletion of nuclear YAP via physiological stimuli, such as substrate stiffness or serum depletion, prior to photoactivation. On a stiff substrate in presence of serum, optoYAP will be nuclear prior to photoactivation, and thus, photoactivation will have no significant effect. Upon successful depletion of nuclear YAP prior to activation, however, it can trigger efficient changes in downstream signaling as shown above. Successful depletion and subsequent photoactivation can be monitored by fluorescence of the GFP fused to optoYAP. Although our results are limited to cell culture—specifically HeLa and A431 cells ([Figures 3, S14, and S15](#))—the underlying method of genetic insertion of an artificial amino acid has been applied to zebrafish ([Liu et al., 2017](#)) and mice ([Ernst et al., 2016](#)). Hence, in principle, the tool should be applicable to investigations in animals as well.

Resource availability

Lead contact

Further information and requests for resources and reagents should be directed to and will be fulfilled by the lead contact, Hanna Engelke (hanna.engelke@uni-graz.at).

Material availability

All unique reagents (optoYAP plasmid) generated in this study are available from the lead contact.

Data and code availability

Data and codes that support the findings of this study are available from the authors upon reasonable request.

METHODS

All methods can be found in the accompanying [Transparent methods supplemental file](#).

SUPPLEMENTAL INFORMATION

Supplemental information can be found online at <https://doi.org/10.1016/j.isci.2021.102185>.

ACKNOWLEDGMENTS

We thank Valerie M. Weaver for helpful discussions and Jana Peliskova for experimental support. This study was funded by the Deutsche Forschungsgemeinschaft (Project ID 201269156 – SFB 1032, project B08 and B11, the excellence cluster NanoInitiative Munich and project PL 696/4-1) and by the Fritz Thyssen Stiftung.

AUTHOR CONTRIBUTIONS

B.I. and H.E. conceived and designed the study; B.I. performed experiments; A.F. and E.P. performed high-resolution microscopy of spheroids; F.G. performed DNA damage experiment and provided support with functionality assays; S.Z. and A.M.V. helped to design the experiments and provided support with functionality assays; H.E. supervised the study. All authors contributed to writing the manuscript.

DECLARATION OF INTERESTS

The authors declare no competing interests.

Received: October 28, 2020

Revised: January 14, 2021

Accepted: February 9, 2021

Published: March 19, 2021

REFERENCES

- Dupont, S., Morsut, L., Aragona, M., Enzo, E., Giulitti, S., Cordenonsi, M., Zanconato, F., Le Digabel, J., Forcato, M., Bicciato, S., et al. (2011). Role of YAP/TAZ in mechanotransduction. *Nature* 474, 179–183.
- Elosegui-Artola, A., Andreu, I., Beedle, A., Lezamiz, A., Uroz, M., Kosmalka, A., Oria, R., Kechagia, J., Rico-Lastres, P., Le Roux, A., et al. (2017). Force triggers YAP nuclear entry by regulating transport across nuclear pores. *Cell* 171, 1397–1410.e14.
- Engelke, H., Chou, C., Uprety, R., Jess, P., and Deiters, A. (2014). Control of protein function through optochemical translocation. *ACS Synth. Biol.* 3, 731–736.
- Ernst, R., Krogager, T., Maywood, E., Zanchi, R., Beránek, V., Elliott, T., Barry, N., Hastings, M., and Chin, J. (2016). Genetic code expansion in the mouse brain. *Nat. Chem. Biol.* 12, 776–778.
- Gautier, A., Nguyen, D., Lusic, H., An, W., Deiters, A., and Chin, J. (2010). Genetically encoded photocontrol of protein localization in mammalian cells. *J. Am. Chem. Soc.* 132, 4086–4088.
- Gegenfurtner, F., Jahn, B., Wagner, H., Ziegenhain, C., Enard, W., Geistlinger, L., Rädler, J., Vollmar, A., and Zahler, S. (2018). Micropatterning as a tool to identify regulatory triggers and kinetics of actin-mediated endothelial mechanosensing. *J. Cell Sci.* 131, jcs212886.
- Lin, C., Pelissier, F., Zhang, H., Lakins, J., Weaver, V., Park, C., and LaBarge, M. (2015). Microenvironment rigidity modulates responses to the HER2 receptor tyrosine kinase inhibitor lapatinib via YAP and TAZ transcription factors. *Mol. Biol. Cell* 26, 3946–3953.
- Liu, J., Hemphill, J., Samanta, S., Tsang, M., and Deiters, A. (2017). Genetic code expansion in zebrafish embryos and its application to optical control of cell signaling. *J. Am. Chem. Soc.* 139, 9100–9103.
- Low, B., Pan, C., Shivashankar, G., Bershadsky, A., Sudol, M., and Sheetz, M. (2014). YAP/TAZ as mechanosensors and mechanotransducers in regulating organ size and tumor growth. *FEBS Lett.* 588, 2663–2670.
- Pocaterra, A., Romani, P., and Dupont, S. (2020). YAP/TAZ functions and their regulation at a glance. *J. Cell Sci.* 133, jcs230425.
- Serra, D., Mayr, U., Boni, A., Lukonin, I., Rempfler, M., Challet Meylan, L., Stadler, M., Strnad, P., Papasaikas, P., Vischi, D., et al. (2019). Self-organization and symmetry breaking in intestinal organoid development. *Nature* 569, 66–72.
- Totaro, A., Panciera, T., and Piccolo, S. (2018). YAP/TAZ upstream signals and downstream responses. *Nat. Cell Biol.* 20, 888–899.
- Valon, L., Marín-Llauradó, A., Wyatt, T., Charras, G., and Treppe, X. (2017). Optogenetic control of cellular forces and mechanotransduction. *Nat. Commun.* 8, 14396.
- Yu, F., Zhao, B., Panupinthu, N., Jewell, J., Lian, I., Wang, L., Zhao, J., Yuan, H., Tumaneng, K., Li, H., et al. (2012). Regulation of the Hippo-YAP pathway by G-protein coupled receptor signaling. *Cell* 150, 780–791.
- Zanconato, F., Cordenonsi, M., and Piccolo, S. (2016). YAP/TAZ at the roots of cancer. *Cancer Cell* 29, 783–803.

iScience, Volume 24

Supplemental information

**Spatio-selective activation of nuclear translocation
of YAP with light directs
invasion of cancer cell spheroids**

Bernhard Illes, Adrian Fuchs, Florian Gegenfurtner, Evelyn Ploetz, Stefan Zahler, Angelika M. Vollmar, and Hanna Engelke

Transparent Methods

1. Plasmid construction of optoYAP

1.1 PCR

Plasmids for optoYAP and optoYAP(Ser127Ala) were obtained as follows: GFP was subcloned into a GFP-hYAP1 plasmid on a pEGFP backbone to yield a 2xGFP-YAP fusion. Subsequently, the optoNLS from the optoNLS-TEV plasmid (Engelke et al., 2014) was prepended. Finally, the mutation Ser127Ala was introduced using the QuikChange kit (Agilent). All cloning steps except for the mutation were performed using standard protocols of the sequence and ligation independent cloning method (SLIC), which has been introduced by Li et al. (Li et al., 2007; Li et al., 2012). QuikChange was performed according to the manufacturer's manual.

The PAG plasmid for the insertion of the photocaged lysine was a gift from the Deiters lab (Engelke et al., 2014).

Primers for Cloning:

2xGFP-YAP:

Insert Forward ACAGGATCCCCGCATCTAGGCGCCGGCCGGATCCT

Vector Reverse: CCGGCCGGCGCCTAGATGCGGGGATCCTGTACAAT

Vector Forward: GCCAACCTGCCGGCCATGGATCCCGGGCAGCAGCC

Insert Reverse CTGCCCGGGATCCATGGCCGGCAGGTTGGCAGCGC

optoYAP:

Insert Reverse: GCCCTTGCTACCATGCCACGGCTCTTGGTATATA

Vector Forward: ACCAAGAGCCGTGGCATGGTGAGCAAGGGCGAGGA

Insert Forward: CTACCGGTCGCCACCCCGGTCGCCACCATGGTGAG

Vector Reverse: CATGGTGCGACCGGGGTGGCGACCGGTAGCGCTA

Primer for QuikChange to optoYAP(S127A):

Forward: TCGAGCTCATgCCTCTCCAGC

Reverse: ACATGCTGTGGAGTCAGG

1.2 OptoYAP Sequencing

Plasmid sequencing was performed by *Eurofins Genomics*.

Primers were ordered from *Metabion*.

Mutation Sequencing Primer:

GCTCTTCAACGCCGTCATGAAC

2. Synthesis and characterization of the caged Lysine

Synthesis of the caged lysine was performed as described in Gautier et al., 2010: 1-(6-Nitrobenzo[d][1,3]dioxol-5-yl)ethanol (500 mg, 2.36 mmol) and Na₂CO₃ (247 mg, 2.36 mmol) were added to THF (5 mL) and cooled to 0 °C under stirring. Next, triphosgene (701 mg, 2.36 mmol) was added to the suspension and the reaction was kept stirring overnight at RT. The reaction was centrifuged to remove Na₂CO₃ and the liquids were subsequently evaporated without heating. The residue was dried under vacuum, to yield a greyish solid (644 mg, 2.36 mmol). NMR confirms the successful synthesis of 1-(6-nitrobenzo[d][1,3]dioxol-5-yl)ethyl carbonochloridate (Fig. S1).

*N*ε-Boc-lysine (500 mg, 2.02 mmol) was dissolved in THF/1 M NaOH (aq.) (1:4 mixture, 8 mL total) under stirring and the solution was cooled to 0 °C. Next 1-(6-nitrobenzo[d][1,3]dioxol-5-yl)ethyl carbonochloridate (496 mg, 1.82 mmol) was added and the reaction was stirred overnight, at RT. The aqueous layer was washed with Et₂O (5 mL) and subsequently acidified with ice-cold 1 M HCl (20 mL) to pH 1 and then extracted with EtOAc (30 mL). The organic layer was dried over Na₂SO₄, filtered, and the volatiles were evaporated, leaving a yellow foam. The yellow foam was dissolved in DCM:TFA (1:1 mixture, 14 mL total) and the reaction was allowed to stir for 40 min. The volatiles were subsequently evaporated and the residue was redissolved in MeOH (5 mL) and precipitated into Et₂O (250 mL), yielding a white solid (679 mg, 1.42 mmol). NMR confirmed the successful synthesis of (2*S*)-2-(*tert*-Butoxycarbonylamino)-6-[1-(6-nitrobenzo[d][1,3]dioxol-5-yl)ethoxy]carbonylaminohexanoic acid which will be called caged lysine from now on (Fig. S2). For use on cells 100 mg of the caged lysine were dissolved in 1 mL H₂O and filtered with a 0.2 μm syringe filter to avoid contamination.

3. Cell Culture and optoYAP Functionality Assays

All cell experiments were prepared in a *Hera-Safe* cell culture unit from *Heraeus*. The cells were incubated in *Hera Cell incubators* also from *Heraeus*. The cells were cultured in DMEM with 10% FBS and 1% Penicillin/Streptomycin at 37°C/5% CO₂.

Experiments in which cells were not embedded in collagen gels or seeded on matrigel were performed in FBS-free DMEM to keep YAP in the cytosol prior to the photo-activation.

Experiments with cells in collagen gel or on matrigel were performed in the presence of FBS as the gels were sufficiently soft to prevent a nuclear localization of YAP even in the presence of FBS.

Cells were either seeded into *ibidi* 8-well, 6-well plates, or *Corning* 96-well plates.

Standard cell numbers for experiments were 5000 cells per well unless noted otherwise.

3.1 Transfection experiments

Transfections of cells in 8-wells plates were carried out by preparing an Optimem solution containing optoYAP plasmid (1 ug/100 µL), PAG plasmid (1 ug/100 µL) and the Xtreme Gene 9 Transfection reagent (3 µl/100 µL). After mixing carefully by tapping against the tube, the solution was then incubated at RT for 20 min. For each 8-well 10 µL of the transfection mixture were used and 3 µL of the caged Lysine were added before incubation. For the luciferase assay (1 ug/100 µL) of the 8xGTIIIC-luciferase plasmid was added as well.

Transfections in 96 well plates used 5 µL of the transfection mixture and 1 µL of the caged lysine per well.

The transfection procedure for single cells and spheroids was carried out in the same manner.

3.2 Photo-activation

For non-directed photo-activation of optoYAP a *Spectroline E-Series* UV lamp (365 nm, 0.6mW/mm²) was used to illuminate the sample for 20 s. For directed photo-activation a laser (405 nm, integrated in a *Zeiss Observer SD* spinning disk confocal microscope) or LED (365 nm, integrated in a *Nikon Eclipse Ti-E*) regulated to the same output as the UV lamp was used to illuminate the sample for 20 s.

3.3 Spheroid formation

To form spheroids, 500 cells were seeded in each well (100 µL DMEM) of a 96-well plate with ultra-low adhesion and incubated at 37°C/5%CO₂ until the spheroids reached the desired size. Spheroids used for experiments had a diameter of 200-300 µm for HeLa spheroids and 100-150 µm for A431 spheroids. For transferring the spheroids into gels disposable plastic pipettes were used.

3.4 Cell Spheroid/Collagen Gel preparation

150 μ L of collagen (8.36 mg/mL) were prepared in a 1.5 mL Eppendorf-tube on ice and 47.5 μ L PBS and 2.5 μ L 1M NaOH, both pre-cooled to 0°C on ice, were added for each well of an ibidi 8-Well plate. The reagents were mixed by pipetting up and down before applying them to the well. Aggregates were carefully aspirated with a pipette and transferred to the gels (2 per well) for a total volume of 400 μ L. The spheroids were incubated for 24 h at 37°C/5%CO₂ before transfection.

3.5 Spheroid Growth Rate

To compare the growth rate of activated and inactivated optoYAP transfected spheroids, collagen embedded spheroids were imaged before activation of optoYAP and then again after three days of incubation after activation. As a control, non-activated spheroids were measured as well. The growth analysis was performed using *Fiji* by comparing 2D projections of the total area covered by spheroids and cell outgrowths before and after incubation.

3.6 RNA extraction for qPCR

RNA Extraction, purification and cDNA synthesis was carried out according to the instructions provided in the RNeasy Mini Kit from *QIAGEN*.

3.7 Luciferase Functionality Assays

HeLa cells were seeded in a 96-well plate with 5000 cells per well and then transfected with optoYAP and 8xGTIIC-luciferase plasmid. After an incubation of 24 hours, optoYAP was activated and after an additional 24 the *Bright-Glo Luciferase Assay* from *Promega* was carried out according to the instructions provided in the manual. The assays were performed on a *Berthold Tristar² LB 942*. 8xGTIIC-luciferase was a gift from Stefano Piccolo (Addgene plasmid # 34615 ; <http://n2t.net/addgene:34615> ; RRID:Addgene_34615)

3.8 Proliferation Assay

500 HeLa cells were seeded into each well of a 96-well plate in media without FBS and then transfected with optoYAP after 24 hours. After an additional 24 hours, half of the wells were illuminated with UV light at 365 nm to photo-activate optoYAP. The remaining wells served as the control and were not treated with UV. Afterward, cell images were recorded every 24 hours to observe cell proliferation with and without activation of optoYAP.

4. Fluorescence imaging and staining

4.1 Confocal laser scanning microscopy

High-magnification brightfield and fluorescence microscopy was carried out utilizing a *Zeiss Observer SD* spinning disk confocal microscope with a Yokogawa CSU-X1 spinning disc unit, an oil objective with 63x magnification. For excitation, a 488 nm (GFP) and 561 nm (YAP) were used. Emission was filtered with a BP 525/50 and LP 690/50 filter, respectively. The setup was heated to 37°C and a CO₂ source was provided to keep the atmosphere at 5% for living samples. The images were recorded and processed with the *Zen* software by *Zeiss*.

4.2 High-Throughput Brightfield imaging

The proliferation assay and general spheroid growth quantification measurements were performed with the *ImageXpress Micro XLS* from *Molecular Devices* using an objective with 10x magnification and the resulting images were evaluated with the *MetaXpress* software.

Further image data analysis was performed with *ImageJ/Fiji* (Schindelin et al., 2012). Specific analysis methods are described at the respective assays.

4.3 High-resolution Fluorescence Confocal Microscopy

Imaging was carried out on a confocal scanning microscope (TE 300; Nikon) with mounted bright-field illumination and camera. The two-photon excitation source for Hoechst staining was a fiber-based, frequency-doubled erbium laser (FemtoFiber dichro bioMP; Toptica Photonics) running at 774 nm. The excitation laser line for YAP staining was a DPSS CW laser running at 561 nm (Cobolt Jive 50, Cobolt AB). The laser powers were 3.3 mW at 774 nm and 2.9 μW at 561, measured in front of the microscope entrance. The laser light was coupled into the microscope via a dichroic mirror (Penta Line zt405/488/561/640/785rpc; AHF Analysetechnik) that separates laser excitation and fluorescence emission. Scanning of the sample in 3D was achieved by using an xyz piezo stage (BIO3.200; PiezoConcept). The laser excitation was focused onto the sample with a 60x (water) 1.20-NA plan apochromat objective (Plan APO VC 60x 1.2 NA, Nikon). The emission was collected by the same objective and spectrally separated by a 647-nm dichroic mirror (BS 647 SP; AHF Analysetechnik). The emission was recorded with two APD detectors (Count Blue; Count Red; Laser Components) and its photons stream registered using a TCSPC card (TH260 pico dual; PicoQuant GmbH). The filter sets for the red APD were: 710/130 bandpass fluorescence filter (HQ 710/130 M; AHF Analysetechnik) and a 750 shortpass (FES0750; Thorlabs GmbH) to additionally block the 774 nm laser line. The filter sets for the blue APD were: 692/40 bandpass fluorescence filter (692/40 BrightLine HC; AHF Analysetechnik) and a 680 shortpass (HC 680/SP; AHF Analysetechnik) to additionally block the 774-nm laser line. The experiment was controlled using a home-written program written in C#. The confocal data was extracted and evaluated afterward by PAM (Schimpf et al., 2018) and ImageJ2 (Schindelin et al., 2012).

4.4 Antibody Staining

Primary and secondary antibodies for were purchased *as stated in the following list*.

List of used antibodies:

YAP

- YAP1 polyclonal rabbit antibody; PA1-46189 *Thermo Fisher Scientific*.
- Donkey anti-Rabbit IgG (H+L) Highly Cross-Adsorbed Secondary Antibody, Alexa Fluor 546; A-10040 *Thermo Fisher Scientific*.

RPA2

- RPA32/RPA2 mouse monoclonal antibody; ab2175, *Abcam*
- Goat anti-Mouse IgG (H+L) Highly Cross-Adsorbed Secondary Antibody, Alexa Fluor 488; A-11001 *Thermo Fisher Scientific*.

gH2A.

- gH2A.X rabbit antibody; 2577 *Cell Signaling Technology*
- Goat anti-Rabbit IgG (H+L) Highly Cross-Adsorbed Secondary Antibody, Alexa Fluor 647; A-21245 *Thermo Fisher Scientific*.

4.5 2D Antibody Staining

HeLa cells were seeded on matrigel to prevent the nuclear localization of YAP and transfected with optoYAP 24h after seeding. 24 hours after transfection, cells were illuminated with UV light (365 nm) for 20 s. After another 6-24 h cells were washed with PBS (pH 7.4) before being fixed with 4% PFA for 10 min. Afterwards, cells were washed three times with PBS for 5 min each. Cells were then permeabilized with Triton X-100 (0.15% in PBS) for 10 min and washed with PBS for 5 min an additional three times. Cells were blocked with 1% BSA containing glycine for 30 min before primary antibodies were applied diluted in PBS with 1% BSA (1 µg antibody per well). After 1 h of incubation, at room temperature (or overnight at 4°C) the cells were washed 5 min with PBS three times. Next, the secondary antibodies were applied diluted in 1% BSA. After one hour of incubation the sample was washed again and Hoechst was applied before imaging.

4.6 3D Antibody Staining

HeLa spheroids embedded into collagen were fixed with 4% PFA for 40 minutes and washed with PBS twice for 20 minutes. The cells were permeabilized for 20 minutes with 0.5% Triton X-100 in PBS and subsequently washed with PBS for 30 minutes. The cells were blocked with 1% BSA in PBS overnight. Primary antibodies were diluted 1:100 with 1% BSA in PBS and cells were incubated for 72 hours. Prior to incubation with secondary antibodies (1:200 in 1% BSA), the cells were washed twice with PBS for 30 minutes. The cells were incubated with secondary antibodies for 48 hours. Afterwards, the cells were washed with PBS for 30 minutes and Hoechst 33342 (0.5 µg/ml) for 40 minutes. Prior to imaging, the cells were washed again with PBS for 30 minutes. Finally, the PBS was renewed and kept in the reservoirs during confocal microscopy.

Supplemental Figures

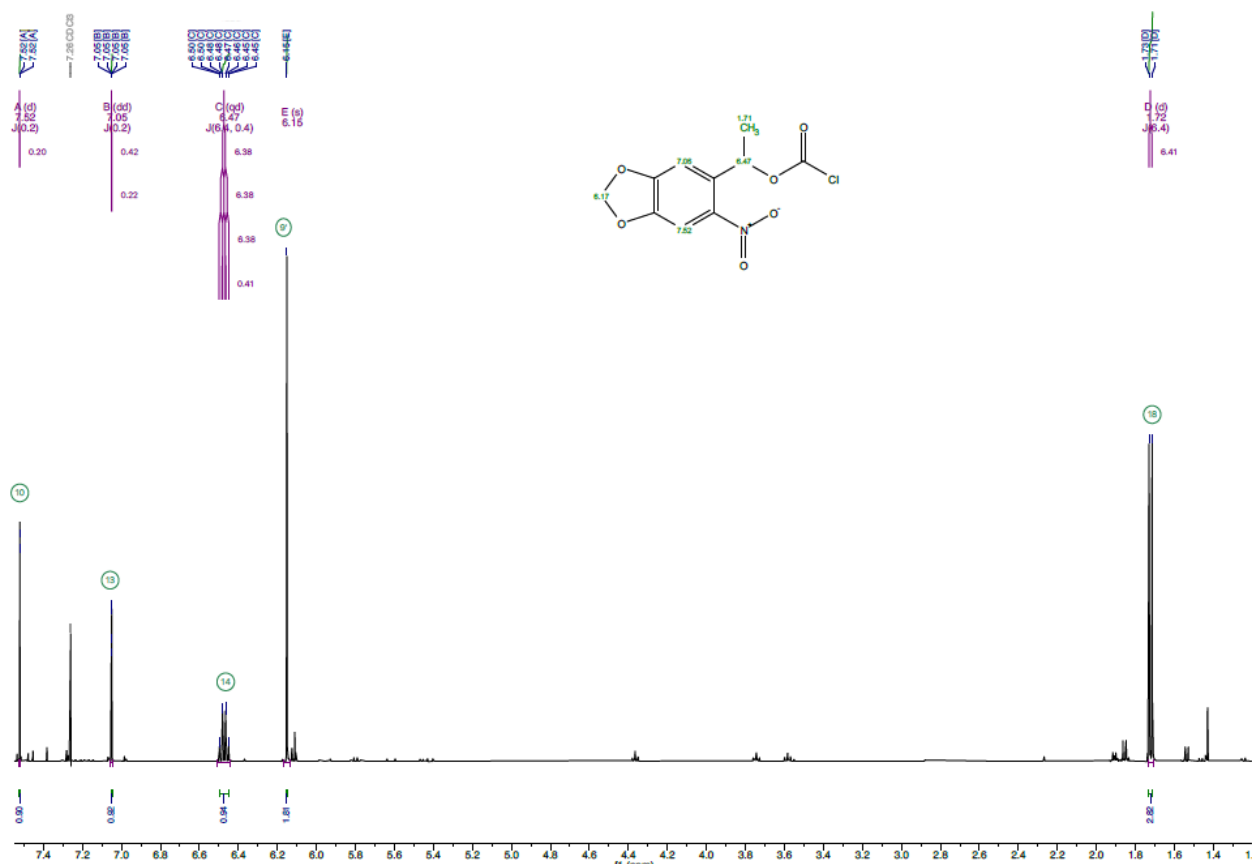


Fig. S1: NMR spectrum of 1-(6-nitrobenzo[d][1,3]dioxol-5-yl)ethyl-carbonochloridate. Related to Figure 1. It is obtained as an intermediate product of the synthesis of the caged lysine. ¹H NMR (400 MHz, CDCl₃): δ (ppm) = 7.52 (d, J = 0.2 Hz, 1 H, H-7), 7.05 (dd, J = 0.2 Hz, 1 H, H-4), 6.47 (qd, J = 6.4, 0.4 Hz, 1 H, H-1'), 6.15 (s, 2 H, H-2), 1.72 (d, J = 6.4 Hz, 3 H, H-2').

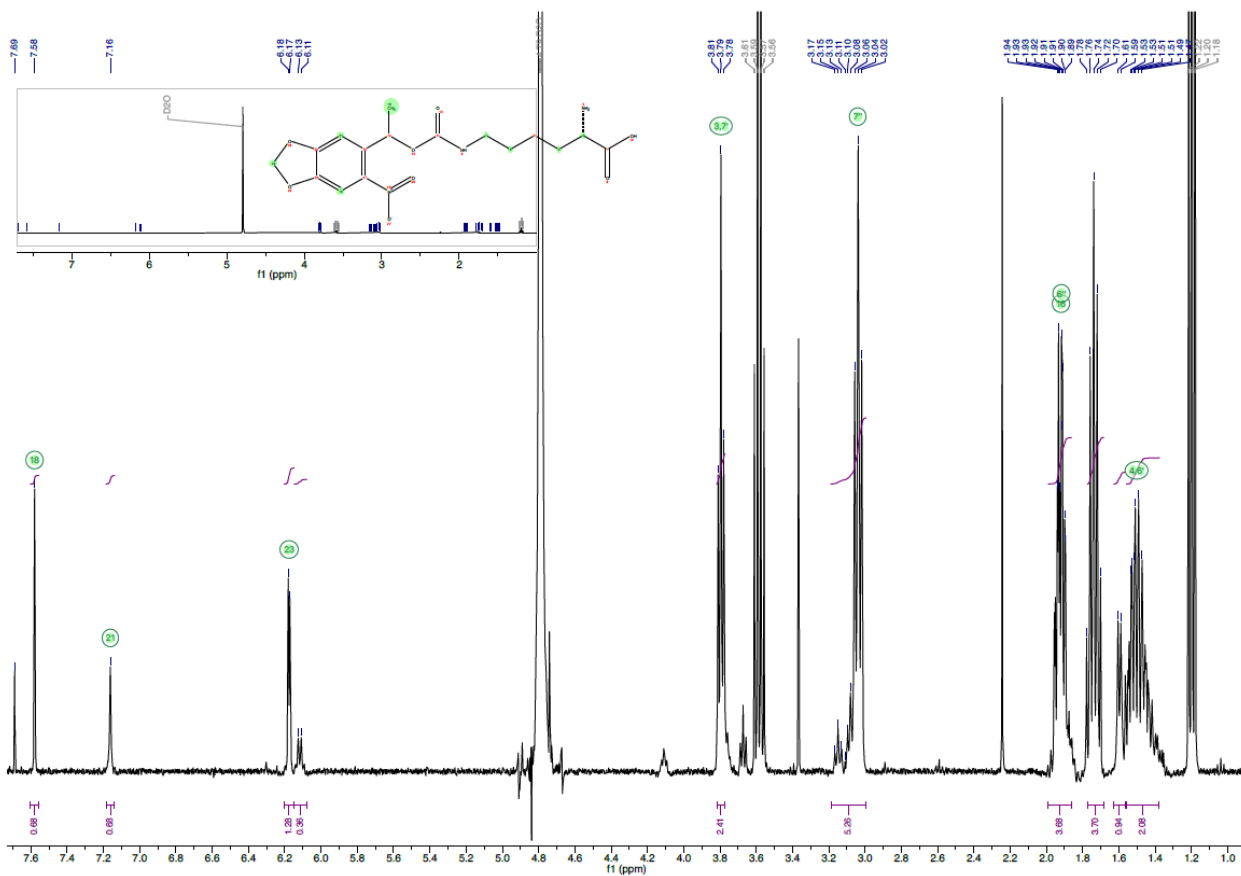


Fig. S2: NMR spectrum of the caged lysine ((2S)-2-(tert-Butoxycarbonylamino)-6-[1-(6-nitrobenzo[d][1,3]dioxol-5-yl)ethoxy]carbonyl-amino-hexanoic acid). Related to Figure 1. ¹H NMR (400 MHz, CDCl₃): (ppm) = 7.58 (s, 1 H, H-7''), 7.16 (s, 1 H, H-4''), 6.18 (d, J = 3.5 Hz, 2 H, H-2''), 6.12 (d, J = 6.4 Hz, 1 H, H-1'), 3.79 (t, J = 6.1 Hz, 2 H), 3.19 – 3.00 (m, 5 H), 1.92 (m, 3 H), 1.62 – 1.38 (m, 3 H).

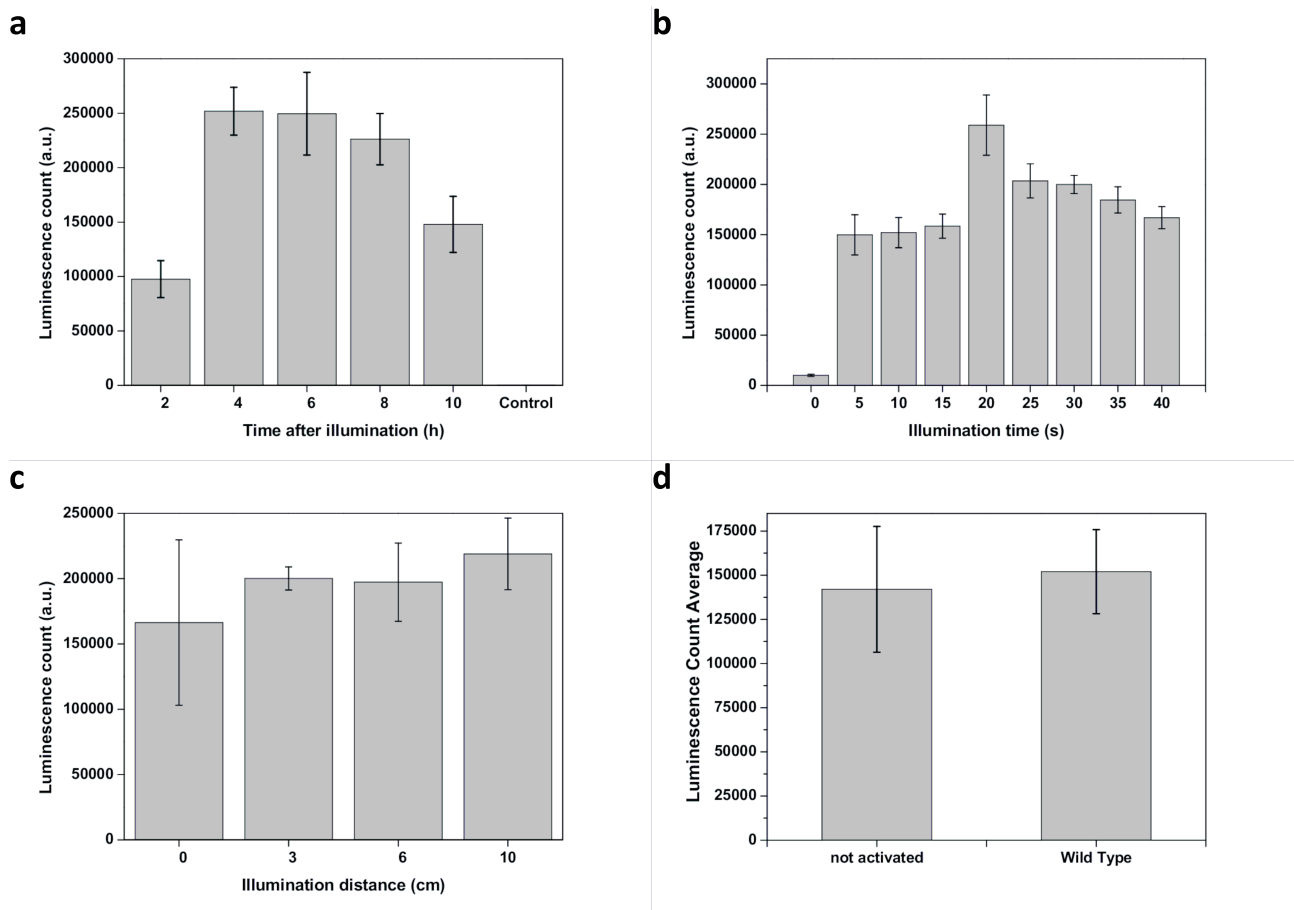


Fig. S3: Luciferase Functionality Assay. Related to Figure 1. a) Time-dependence of optoYAP activity. The observed luciferase count, and thus optoYAP activity, is time-dependent. Measurements taken at different time points after illumination show a clear maximum in activity at 4 to 6 h after photo-activation with a steady decline afterward. b) Dependence of optoYAP activity on illumination time. To gauge the effect of variations in illumination time on optoYAP activity, transfected HeLa cells were illuminated for different time periods to photo-activate optoYAP. Subsequently, the corresponding luciferase activity was recorded. The results show a clear peak in luciferase count and thus YAP activity at an illumination time of 20 seconds. c) Distance dependence of the photo-activation: The distance between light source and sample during photo-activation and thus the power needed to activate optoYAP was investigated. Photo-activation was performed at the indicated distances between light source and sample and the subsequent luciferase activity was recorded. While there was a slight deviation in recorded luminescence in case of full contact of the UV light to the sample (0 cm distance), no significant differences could be observed for larger distances. The luciferase activity shows thus little sensitivity to deviations in light intensity of the UV light source. d) Comparison of luciferase activity of optoYAP transfected, non-activated cells (not activated) and cells that were not transfected with optoYAP and not activated (Wild Type) shows that optoYAP transfection does not influence downstream signaling significantly prior to photoactivation. Data in all figures are represented as mean +/- standard deviations of triplicates.

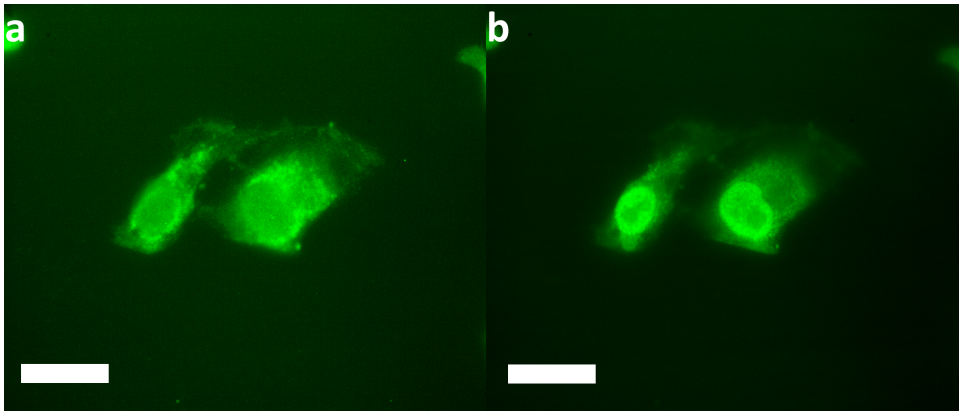


Fig. S4: optoYAP translocation. Related to Figure 1. optoYAP transfected HeLa cells on a thin layer of matrigel before (a) and 30 min (b) after illumination. Scale bar: 20 μ m.

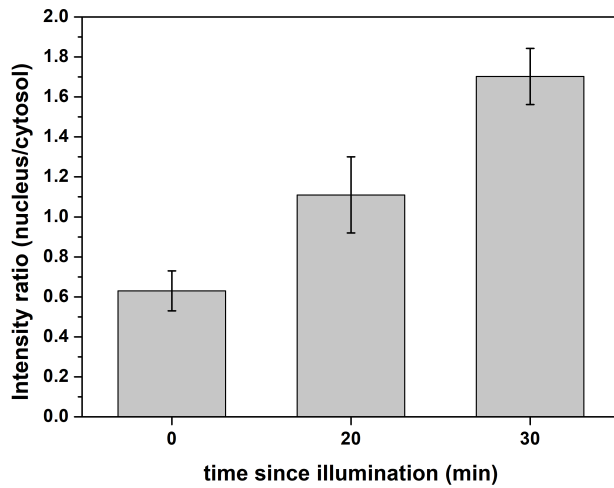


Fig. S5: Kinetics of optoYAP translocation. Related to Figure 1. Intensity ratio of (nucleus/cytosol) of optoYAP in HeLa cells in 2D cell culture at different times after optoYAP activation. Prior to activation the optoYAP signal is localized in the cytosol, but gradually translocates into the nucleus upon activation. Note: images are not background corrected for analysis, thus leading to an intensity ratio above zero before illumination, and above 1 after illumination. Data are represented as mean \pm standard deviations of triplicates.

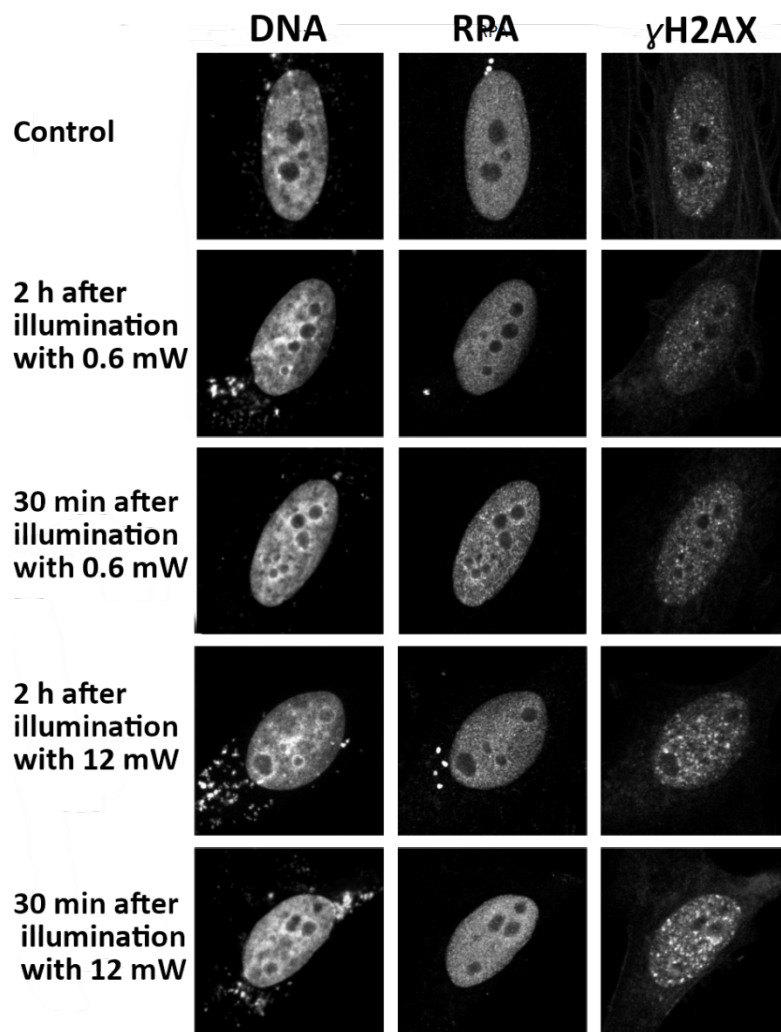


Fig. S6: Assessment of the damage caused during photo-activation with 20 s UV light (365 nm) illumination. Related to Figure 1. HeLa cells were seeded on an 8-well microscopy slide and transfected with optoYAP. After photo-activation at different intensities the damage to the cells was investigated with markers for DNA and as a marker of DNA damage with the DNA damage repair proteins RPA and γ H2AX. Comparing the activated samples to a transfected non-activated control shows that the higher intensity leads to some DNA damage (visible by an increase in RPA and γ H2AX signal) that is almost repaired after 2 h. The lower intensity of 0.6 mW leads to negligible DNA damage, which cannot be detected anymore after 2h. Thus, this intensity was chosen for all experiments.

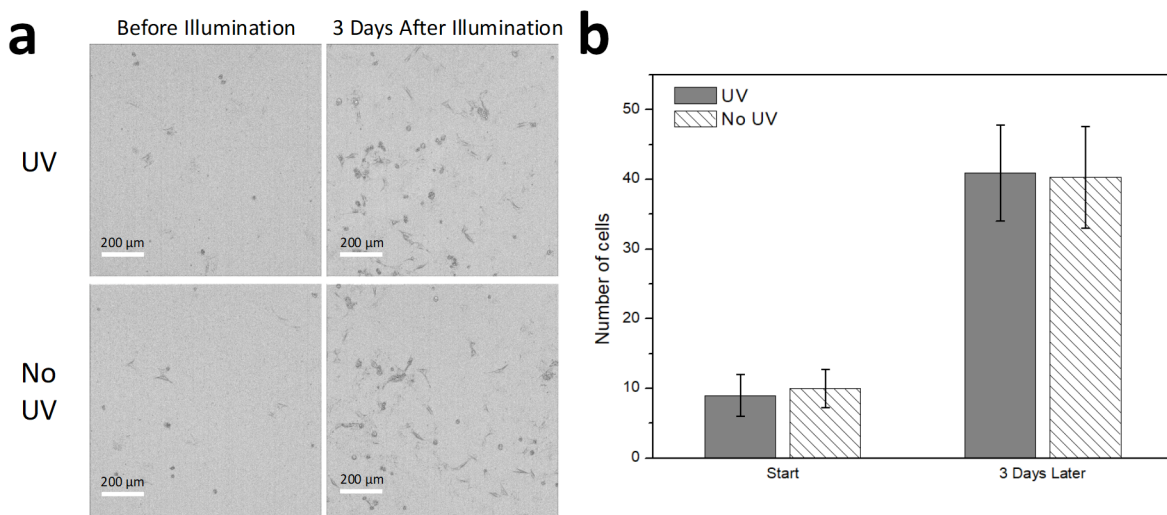


Fig. S7: Effect of UV illumination on proliferation. Related to Figure 1 and 2. Proliferation of cells is not affected by the illumination used for optoYAP activation. a) Brightfield microscopy images of cells at the time of illumination and 3 days later. The upper row was illuminated with UV as used for optoYAP activation and the lower row serves as control, which was not illuminated. Scale bar: 200 μm . b) Quantitative analysis of the number of cells at the time point of UV-illumination and 3 days later compared to controls, which were not illuminated, shows that proliferation is not influenced by the UV used for photo-activation. Data are represented as mean \pm standard deviation.

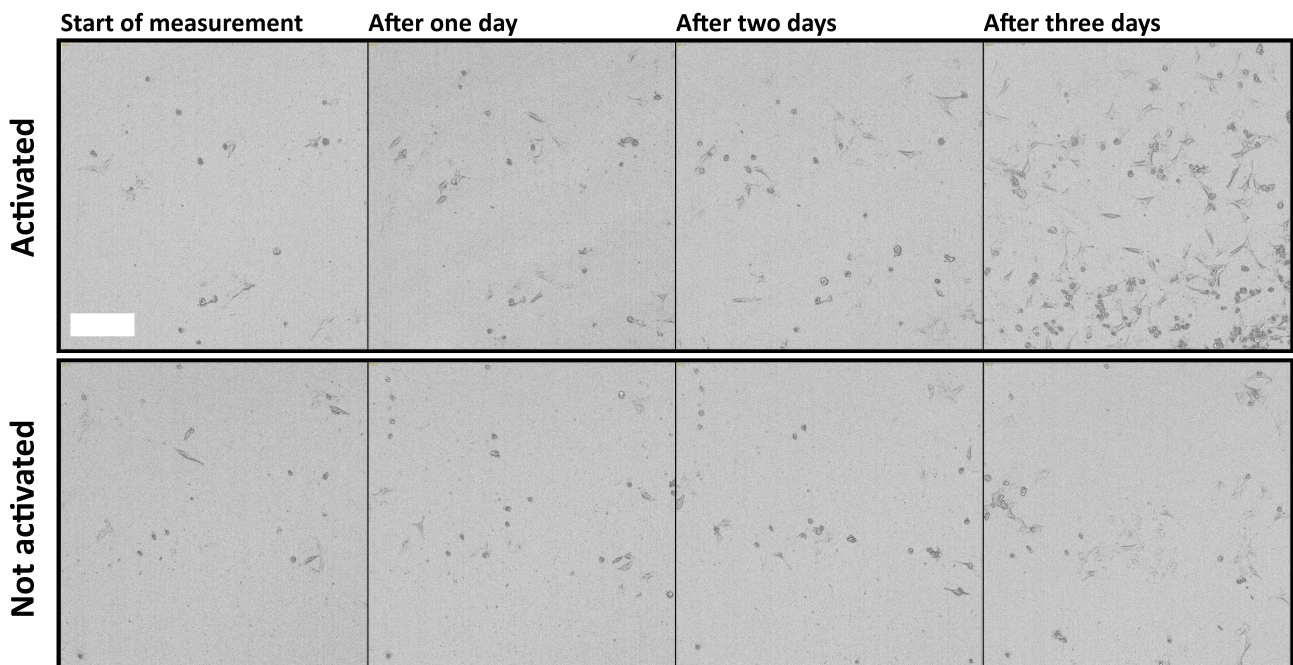


Fig. S8: Proliferation assay on optoYAP-transfected HeLa cells. Related to Figure 2. Time is measured after optoYAP activation. The upper row shows activated cells, the lower row non-activated controls. The images show a clear increase in overall growth upon optoYAP activation. Scale bar: 200 μm .

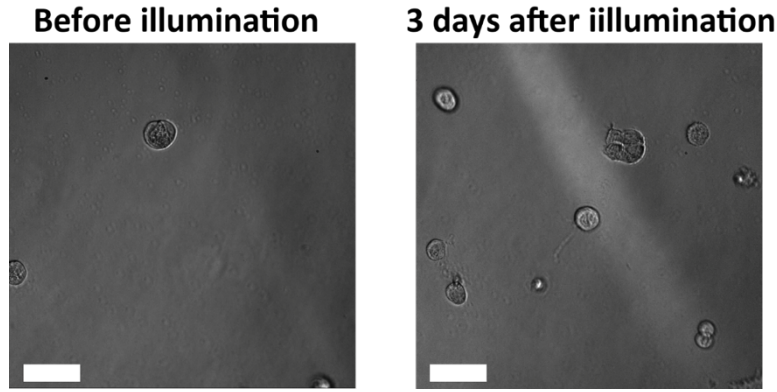


Fig. S9: Morphology of optoYAP transfected HeLa cells on matrigel. Related to Figure 2. OptoYAP transfected HeLa cells on a layer of matrigel before and three days after photo-activation. Cell morphology of transfected cells on matrigel did not change after photo-activation even after several days of incubation. Scale bar: 200 μ m.

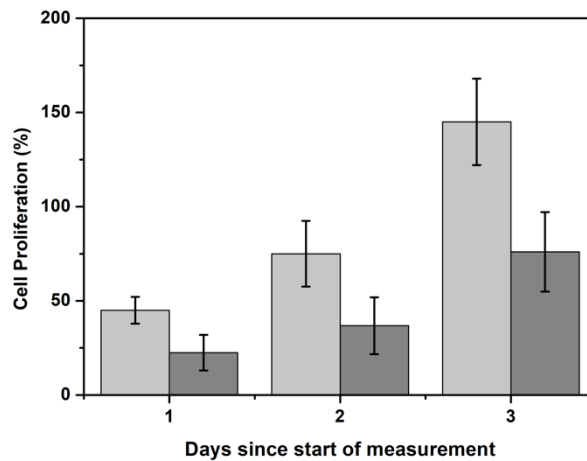


Fig. S10: Effect of optoYAP activation on proliferation on matrigel. Related to Figure 2. Cell proliferation of activated (light grey) and non-activated (dark grey) optoYAP transfected HeLa cells on matrigel in presence of FBS. The overall growth rate on matrigel is about a factor of two smaller in comparison to cell proliferation on a plastic substrate without FBS. Yet, likewise, the activated samples show a strongly increased proliferation compared to the non-activated samples. Data are represented as mean values \pm standard deviations of triplicates.

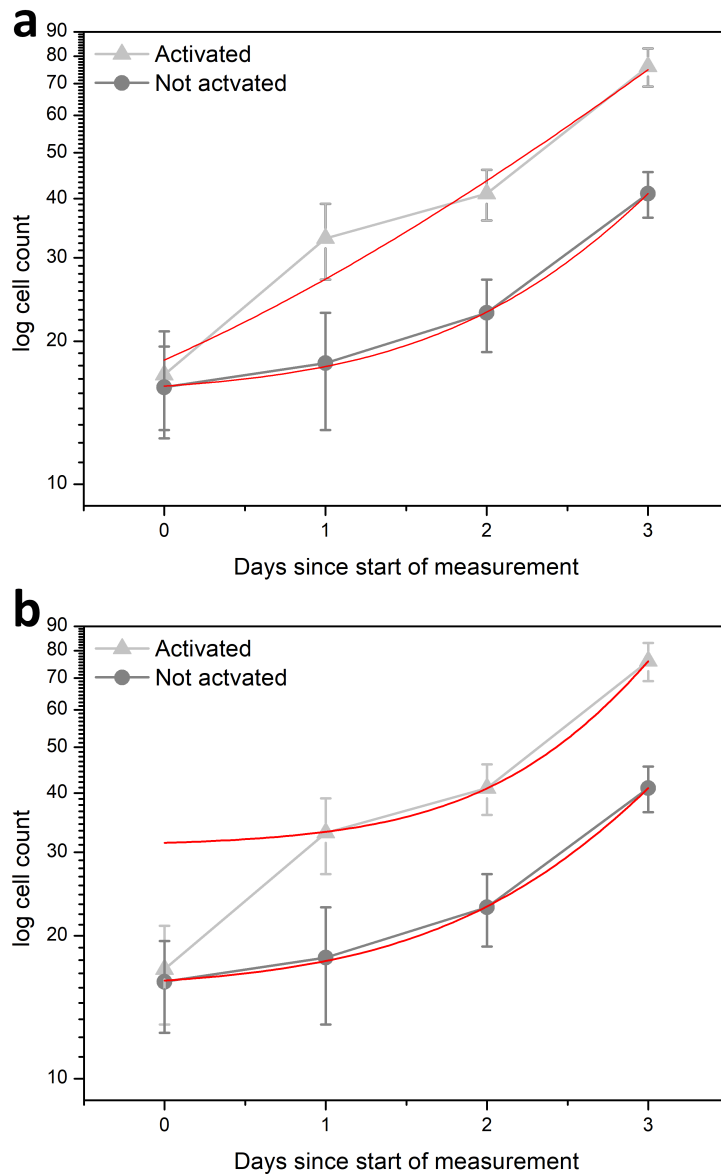


Fig. S11: Analysis of effect of optoYAP activation on proliferation. Related to Figure 2. Logarithmic plot of the cell count with exponential fits. a) Fitting exponential growth curves to the data yields an average growth rate of 0.49/d for activated and 0.31/d for non-activated cells indicating the increase in growth upon optoYAP activation. However, due to the apparent reduction in growth rate of the activated sample after day 1 the fit is only a rough approximation. b) Fitting only the last three data points of the activated sample yields a fit of much better quality and a growth rate of 0.27/d, which is very similar to that of non-activated cells. The strong deviation of the first data point from this curve shows the strongly increased growth during the first 24 h of the experiment. This leads to the conclusion that the observed difference between activated and non-activated samples mainly stems from the cell proliferation of the first day of observation, while the proliferation returns to normal growth rates after the first day. Data are represented as mean values \pm standard deviations of triplicates.

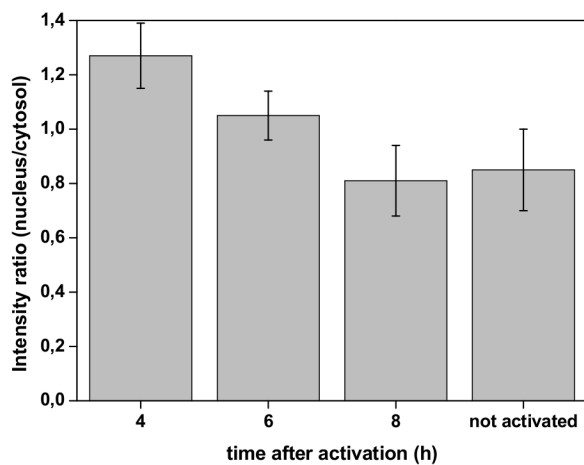


Fig. S12: Intensity ratio of (nucleus/cytosol) for YAP (via antibody staining) in HeLa cells on matrigel at different times after optoYAP activation. Related to Figure 2. 4 h after incubation YAP is in the nucleus followed by a decrease in the ratio of nuclear/cytosolic YAP. Note: images are not background corrected for analysis, thus leading to an intensity ratio above zero before illumination, and above 1 after illumination. Specifically due to the cell morphology on matrigel, the nuclear background signal is quite high. Data are represented as mean +/- standard deviations.

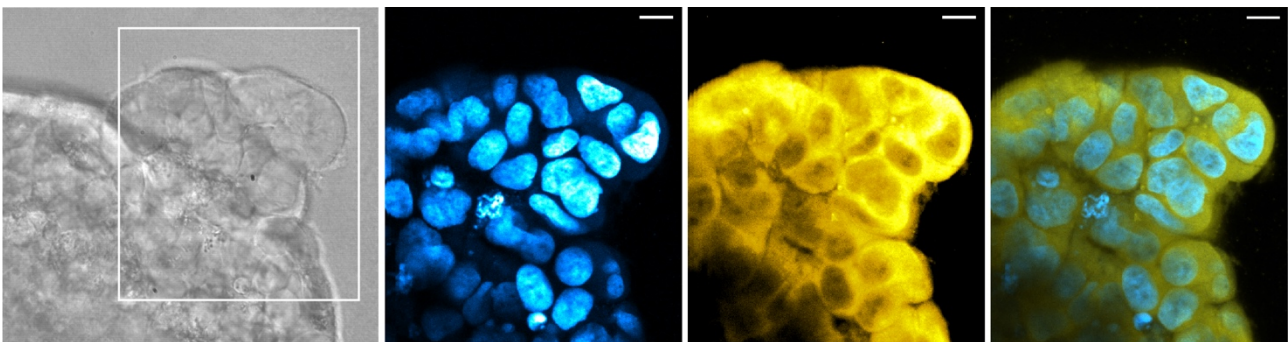


Fig. S13: High resolution confocal microscopy image of the inside of a fixed HeLa spheroid transfected with optoYAP. Related to Figure 3. The spheroid is embedded in a collagen gel and was completely illuminated for activation. The spheroid was fixed 3 days after activation. YAP appears concentrated in the cytosol. Scale bars: 5 μ m.

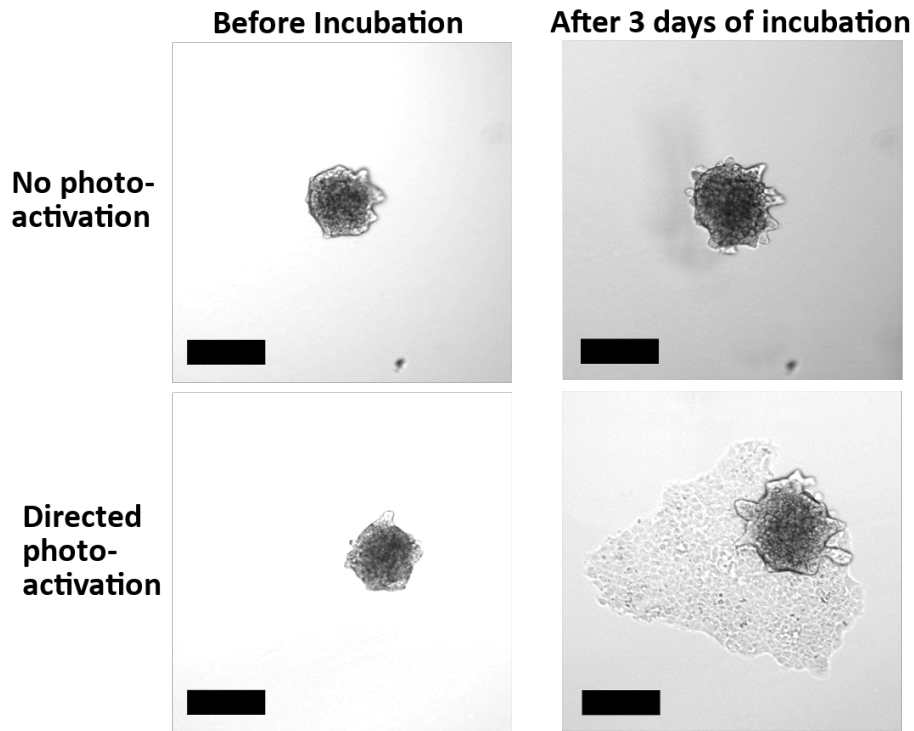


Fig. S14: optoYAP transfected A431 spheroids embedded into collagen gel. Related to Figure 3. To investigate if the effects of optoYAP activation can also be observed in other cell lines, A431 spheroids were transfected according to the same protocol described for HeLa spheroids and selectively activated. The treated A431 spheroids showed similar results to those obtained from HeLa spheroids: non-activated samples exhibit no discernible invasive behavior aside from general growth of the spheroid, while activated samples show significant invasion starting from the activated area. Scale bars: 150 μm .

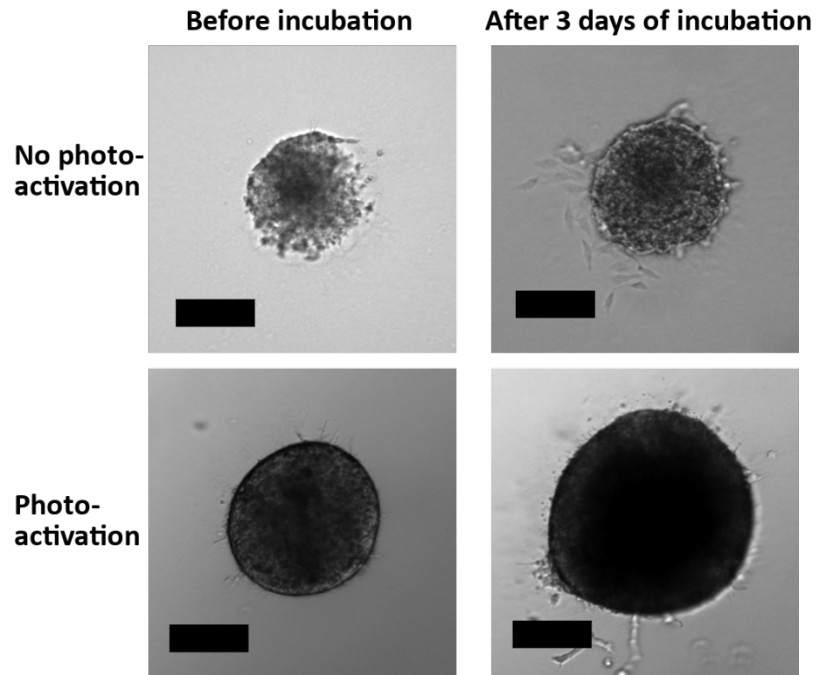


Fig. S15: Non-transfected HeLa spheroids embedded in collagen gel. Related to Figure 3. To investigate if the observed behaviors of the treated HeLa spheroids are indeed caused by optoYAP, non-transfected HeLa spheroids were used as controls and activated the same way as optoYAP. Neither the activated nor the non-activated samples show invasive behavior comparable to that of the optoYAP transfected spheroids. The only discernible difference between before and after incubation is an increase in overall spheroid size in both cases – with and without activation. Scale bars: 100 μm .

Supplemental references

- Engelke, H., Chou, C., Uprety, R., Jess, P. and Deiters, A. (2014). Control of protein function through optochemical translocation. *ACS Synth Biol* 3, 731-736.
- Li, M.Z. and Elledge, S.J. (2007). Harnessing homologous recombination in vitro to generate recombinant DNA via SLIC. *Nat. Methods* 4, 251-256.
- Li, M.Z. and Elledge, S.J. (2012). SLIC: a method for sequence- and ligation-independent cloning. *Methods Mol. Biol.* 852, 51-59.
- Schindelin, J., Arganda-Carreras, I., Frise, E., Kaynig, V., Longair, M., Pietzsch, T., Preibisch, S., Rueden, C., Saalfeld, S., Schmid, B. et al. (2012). Fiji: an open-source platform for biological-image analysis. *Nat. Methods* 9, 676-682.
- Schrimpf, W., Barth, A., Hendrix, J. and Lamb, D.C. (2018). PAM: A Framework for Integrated Analysis of Imaging, Single-Molecule, and Ensemble Fluorescence Data. *Biophys. J.* 114, 1518-1528.